Journal of
Computational and Theoretical Nanoscience
Vol. 10,534-547,2013

RESEARCH ARTICLE

Coupled Magneto-Thermo-Electromechanical Effects and Electronic Properties of Quantum Dots

Sanjay Prabhakar[1*], Roderick V. I\l. Melnik[12'3'4], Pekka Neittaanmaki[2], and Timo Tiihonen[2]

[1]M[2]NeT Laboratory, Wilfrid Laurier University, Waterloo, Ontario N2L 3C5, Canada
[2]Department of Mathematical Information Technology, University of Jyvaskyla, 40014, Finland
[3] Basque Excellence Research Center BCAM, 48009, Bilbao, Spain
[4]Ikerbasque, Basque Foundation for Science, 48011, Bilbao, Spain

For the first time, we systemically analyze the influence of magneto-thermo-electromechanical effects on the band structure calculations by using the fully coupled model. We focus on three different types of quantum dots (QDs): (a) ferroelectric, (b) piezomagnetic, and (c) magnetoelectric, with and without wetting layers (WLs). We demonstrate that the influence of such coupled effects in the general fully coupled framework for studying properties of QDs can be significant and we quantify these effects in each case. For example, in magnetic GaN/$BaTiO_3$ QDs, we found that the influence of electromechanical effects on the band structure calculations and the spin splitting energy are practically independent of temperature. However, in piezoelectric AIN/GaN QDs, the influence of temperature on the electromechanical effects, electronic properties and spin splitting energy is significant. In particular, in piezoelectric AIN/GaN QDs, the intra-subband energy (i.e., the energy difference between ground and first excited states) decreases with the increase in temperature.

Keywords: Quantum Dots, Coupled Magneto-Thermo-Electromechanical Effects, Ferroelectric, PiezdSa^i^ie^otr^^iOfifelJ&Hc8^r^- &tYucture Calculation, Qu$_a$ntum-cta0mfe^{can} Scientific Publishers

1. INTRODUCTION

It has been known that both strain and such fields as magnetic, thermal, electromechanical can be used as tuning parameters for the optical response of Low Dimensional Semiconductor Nanostructures (LDSNs) in photonics, band gap engineering, optoelectronics and other applications.[1-5] The combined influence of these fields in the magnetic QDs can lead to their significant contributions in band structures of LDSNs used at the device level (e.g., nonvolatile memory devices).[1,2] Furthermore, the investigation of the electron spin splitting energy due to spin-orbit interaction in QDs is also essential.[6-9] These coupled multiphysics effects in properties of QDs grow into a substantial factor to be accounted for in many current and potential applications of optoelectronic devices, as well as in other applications.[1,7,10-15]

Among LDSNs, wide band gap semiconductor nanostructures such as AIN/GaN QDs doped with magnetic materials (e.g., Mn or Cr), have attracted significant attention due to their current and potential applications in optical, optoelectronic and electronic devices used in nano- and bionano-technological applications.[16-19] Several other classes of LDSNs also present significant interest for applications. Indeed, ferroelectric nanostructures such as $BaTiO_3$ or PZT are important for the design of nonvolatile memory density devices, actuators and transducers, etc.[20-24] The class of multiferroic nanostructures provides another important example for applications.[4,25,26]

In these nanostructures, strain is induced due to the lattice mismatch at the interfaces of the heterojunction that can be used to design new promising devices such as spintronic.[8,27-35] Al±ough some coupled effects were included in the study of LDSNs (e.g., Refs. [10,29]), the influence of coupled magneto-thermo-electromechanical effects has not been studied systematically.

Another point to note is that the Rashba spin-orbit coupling can be used as a key parameter in controlling the electron spin in AIN/GaN QDs.[8,36] The mathematical expression for the Rashba spin-orbit coupling (given later in this paper in Eq. (22)) is well established for semiconductor heterojunction-type devices.[11,37] In several recent works, the Rashba spin-orbit coupling in QD systems was explored by several different groups (see Refs. [38—42]). However, the influence of the coupled magneto-thermo-electroelasticity in QDs has been largely neglected in the

* Author to whom correspondence should be addressed.

 1546-1955/2013/10/534/014 doi: 10.1166/jctn.2O13.2731

literature and we intend to cover this gap. In this context we mention Ref. [43] where the authors studied the electronic properties of AlGaN/GaN/$BaTiO_3$ double heterostructures by combining first principles and charge control method. Our approach developed here is different from earlier studies (e.g., Ref. [43]). We investigate the influence of magneto-thermo-electromechanic al effects on the ferroelectric, piezomagnetic and magnetoelectric QDs based on the fully coupled quantum-continuum models implemented via the finite element methodology.[44]

Various approaches such as atomistic, pseudopotential, and tight binding have been applied to investigate the optical and electronic properties of LDSNs.[45^8] In this paper, we apply the $k \cdot p$ methodology which allows us to incorporate electromechanical and other coupled effects in the band structure calculations of QDs in a straightforward manner.-®'-*

In what follows, we undertake a systematic study of the coupled effects of magneto-thermo-electroelasticity in three different types of nanostructures: (a) ferroelectric (b) piezomagnetic (multiferroic, magnetostrictive) and (c) magnetoelectric. We also present a numerical analysis of these effects on the electronic properties of QDs.

The rest of the paper is organized as follows. In Section 2, we provide details of the models to account for the influence of electromechanical effects on the properties of wu rtzi te QD stru ctures. We al so provide thei r generali zations to the coupled magneto-thermo-electroelasticity. Section 3, we give details of the total Hamil^nilS^ft^'.^^^S&S^- 0?. Mar ^919, ing classical and quantum parts. In SectuS/^Twe prMenf^ the developed mathematical models in cylindrical coordinates to study the magneto-thermo-electromechanical effects on the band structures of wurtzite QDs. Section 5 presents a series of numerical results demonstrating the influence of magneto-thermo-electromechanical effects on the properties of ferroelectric, piezomagnetic and magnetoelectric QDs. Finally, Section 6 summarizes our findings.

2. COUPLED EFFECTS IN QUANTUM DOTS

In this section, we provide details of a mathematical model to study the influence of magneto-thermo-electromechanical effects on the properties of wurtzite QD structures.

2.1. Balance Equations for Mechanical, Electric and Thermal Fields

Following Refs. [29,49,50], a coupled system of mechanical, electrostatics and thermal energy balance equations to study thermo-electromechanical effects in QDs with axial symmetry can be written as:

$$\sigma_{ij,j} + f_i = 0 \tag{1}$$

$$Dt.i \sim q = 0 \tag{2}$$

$$h_{i,t} . - k = 0 \tag{3}$$

Here cr$_{ij}$- are the stress tensor components, D_i are the electric displacement vector components and $h,$- are the heat flux vector components. Also, f are the components of body mechanical forces, q is the electric charge and k is the heat source. Constitutive equations for the system (l)-(3) in a more general setting are given below, in Section 2.3.

2.2. Gradient Equations

The equations that relate the linear strain (for generalization to nonlinear strain models, see Refs. [28,51-54]) and mechanical displacement, electric field and electric potential, the thermal field and temperature change, are referred to as gradient equations which can be written as,

$$\varepsilon_{kl} \sim \frac{1}{2}(u_{k,l} + u_{l,k}) \tag{4}$$

$$Ek = \sim Vk \tag{5}$$

$$\wedge k \sim \sim \beta k \tag{6}$$

$$Qk \sim \sim \mathbb{R}k \tag{7}$$

where e_{kl} are the strain tensor components, E_k is the electric field vector, Q_k is the thermal field vector, u is the mechanical displacement vector, V_k is the electric potential and $0_{/c}$ is the change in temperature from the reference

2.3. Fully Coupled Magneto-Thermo-Electromechanical System

The coupled system of magneto-thermo-electroelasticity including the Navier and Maxwell's equations that account for the piezoelectric field[55] can be written as

$$\partial_j \sigma_{ik} = 0 \tag{8}$$

$$djDt = 0 \tag{9}$$

$$\partial_i H_i = 0 \tag{10}$$

$$\partial_i q_i = 0 \tag{H}$$

The components tz$_{j7c}$, £),, H_t and q_i are coupled via the Helmholtz free energy function:[29]

$$\begin{aligned}\Phi(\varepsilon_{ij}, E_n, \theta, B_p) &= \frac{1}{2}C_{ijkl}\varepsilon_{ij}\varepsilon_{kl} - {}^{e}ijk\wedge i^{\varepsilon}jk \quad - \frac{1}{2}\epsilon_{ij}E_iE_j - \beta_{ij}\Theta\varepsilon_{ij} \\ &\sim Pi^{E}i\mathbb{R} - \quad \frac{1}{2}a_T\Theta^2 + {}^{\wedge V}pq^{B}p^{B}{}_{q} \sim {}^{Ur}pij^{e}ij^{B}p \\ &\text{-}X_{pm}E_mB_p\text{-}T_pB_p\mathbb{R}\end{aligned} \tag{12}$$

where $v_{pq} = i/p_{pq}$ and p_{pq} is the permeability coefficient, ir_{pii} is the piezo-magnetic coefficient, A_{pm} is the electromagnetic coefficient and T_p is the thermo-magnetic

RESEARCH ARTICLE

coupling. Also $a_T = c_e^V/T_{ij}$, and is the heat capacity at constant strain tensor and at constant electric potential. The resulting constitutive equations in this case can be written as:

$$\sigma_{kl} = \left(\frac{d\sigma_{kl}}{d\varepsilon_{kl}}\right)_{E,B,\Theta} = c_{ijkl}\varepsilon_{ij} - e_{mkl}E_m - \pi_{pkl}B_p - \beta_{kl}\Theta \quad (13)$$

$$D_n = -\left(\frac{\partial\Phi}{\partial E_n}\right)_{\varepsilon,B,\Theta} = e_{nij}\varepsilon_{ij} + \epsilon_{mn}E_m + \lambda_{pn}B_p + p_n\Theta \quad (14)$$

$$H_q = \left(\frac{\partial\Phi}{\partial B_q}\right)_{\varepsilon,E,\Theta} = -V q_{ijS}ij \sim \wedge qm^E m + {}^V p_q{}^B p \sim {}^T p^{\&} \mathrm{O}^5)$$

$$s = (-)\left(\frac{\partial\Phi}{d\&}\right)_{eEB} = \beta_{ij}\varepsilon_{ij} + Pn,E_m + r_pB_p + a_T\& \quad (16)$$

where e_{ik} is the piezoelectric coefficient, $e_{/n}$ is the permittivity, P_{sp} is the spontaneous polarization and E_m is the built in piezoelectric field. It is also well known that the internal strain reduces the band gap in semiconductor nanostructures, influencing the quantum confinement effect.[56] In what follows, we apply the Lifshits-Rozentsveig theory that accounts for such strains[57,58] to study the influence of the Cauchy strain and the internal strl£?fi &82t2(Mli1tf^Tili55j{thh: Thu, Q^tM3£s8Q^$iW&il^nter action is an essential ingredient in ^^fa$_{ena\ of\ switching\ electron\ spin\ states}$ in QDs. It can be written as[6,7,36,38]

have the form:

$$\wedge'7\ \text{“}\varepsilon_{ij}^{u}\text{”I”}\ \varepsilon_U^0 \quad (17)$$

where $e?_{ij}$ are the local intrinsic strain tensor components due to lattice mismatch and d_{ij}^u are position dependent strain tensor components. These two can be written as

$$4 = (8_{(}\text{-}8\wedge)< + 8\wedge X \quad (18)$$

$$e_{ii}^{u} = \frac{1}{2}(\partial_j u_i + d_i{}^v j) \quad \mathrm{C}^{19})$$

where $e_{a}^{*} = (a_m - a_{QD}/a_{QD})$ and $e_c^* = (c_{,,,} - c_{QD}/c_{QD})$ are the local intrinsic strains along a and c directions, respectively.[59] Also, a_m, c_m and a_{QD}, c_{QD} are the lattice constants of the matrix and the QD, respectively.

3. HAMILTONIANS OF QUANTUM DOTS ACCOUNTING FOR CLASSICAL AND QUANTUM PARTS

The band diagram calculation of self-assembled QDs requires a solution of the Schrödinger equation supplemented by a system of partial differential equations that account for coupled classical effects. In particular, for epitaxially grown self-assembled QDs in presence of externally applied electric fields, we need special care in the inclusion of electromechanical effects into the Hamiltonian of QDs.[60] In addition, applied magnetic fields must be gauge invariant in the solution of Schrödinger equation to study the spin splitting energy of QDs.[61] We calculate the electronic properties of QDs by using the relativistic $k \cdot p$ envelope function method that up to date has been successfully applied to include the influence of the magnetic[62] and thermo-electromechanical fields[29] separately. The total Hamiltonian of the QDs in this case can be written as

$$H = H_{k\cdot p}^{n\times n} + H_R + H_c^e \quad (20)$$

Here, H_R is the Rashba (Rashba-Bychkov) spin orbit interaction and H_c^* is the strain dependent part of the kinetic energy of the electron to be discussed later. The remaining portion of the Hamiltonian can be written as,

$$H_{k\cdot p}^{n\times n} = p_x\frac{1}{m_e^{\perp}}P + P\frac{1}{m_e^{\perp}}P_x + P_y\frac{1}{m_e^{\perp}}P_y + P_z\frac{1}{m_e^{\parallel}}P_z + E_c(\text{”J} + {}^{eV}(\text{‘e}) + \frac{1}{2}g_0\mu_B B\sigma_z \quad (21)$$

where the kinetic momentum operator $\vec{P} = \vec{p} + e/c\vec{A}$ *is* the sum of the conical momentum operator $\vec{p} = -ih(d_x, d_y, 0)$ and $\vec{A} = (B/2)(-y, x, 0)$ which is the vector potential in symmetric gauge. Here B is the applied magnetic field along z-di recti on, μ_B is the Bohr magneton, $E_c(r_e)$ is the conduction band edge profile and e is the electronic charge. We denote by a, the usual Pauli spin matrix along

$$H_R = \wedge\wedge P_y\text{-}<T_y Pj \quad (22)$$

where a_R is the Rashba coefficient for spin orbit interaction, a_x and a_y are the Pauli spin matrices along x and y-directions.

The strain dependent part of the electron Hamiltonian in (20) can be written as

$$H_c^e = a_c^{\parallel}(r)e_z,(r) + \wedge(r\wedge e\wedge r) + e_{y\}!}(r)J \quad (23)$$

where ojj and $a_c^{\perp}$ are the conduction band deformation potentials along and perpendicular to the symmetric axis.

4. QUANTUM-CONTINUUM MODEL IN CYLINDRICAL COORDINATES AND ITS COMPUTATIONAL IMPLEMENTATION

Based on the coupled model described in Sections 2 and 3, in this section, a general two-dimensional (2D) model in cylindrical coordinates has been developed to study the influence of the magneto-thermo-electromechanical effects on the band structures of QDs having cylindrical symmetry. Examples that follow focus on wurtzite QDs. In this case, with appropriate boundary conditions, the solutions

to Eqs. (8)-(ll) are also axisymmetric.[29,63] Therefore, in this special case, the original 3D problem can be reduced to a 2D problem.[64] The linearly independent elastic constants and piezoelectric constants in a crystal with wurtzite symmetry are given as

$$\text{Cui!} = C_{11},\ C_{1122} = C_{12},\quad = \quad \text{Cl 133} = C_{13},$$

$$C3333 = C33,\quad C_{2323} = C44,$$

$$C2121 = \frac{1}{2}(C_{11} - C_{12}),\quad *311 = *31,$$

$$*333 = *33,\quad *113 = *15,$$

$$\epsilon_{11} = \epsilon_1,\quad \epsilon_{33} = \epsilon_3$$

The magneto-thermo-electromechanical balance equations in cylindrical coordinates for axially symmetric QDs of wurtzite structure can be written as (see e.g., Refs. [28,63,65])

$$\frac{\partial \sigma_{rr}}{dr} + \frac{\partial \sigma_{rz}}{dz} + \frac{\sigma_{rr} - \sigma_{\theta\theta}}{r} = 0 \tag{24}$$

$$\frac{da_{rz}}{dr} + \frac{da_{zz}}{dz} + \frac{1}{r}\sigma_{rz} = 0 \tag{25}$$

$$\frac{dD_r}{dr} + \frac{dD_z}{dz} + \frac{1}{r}D_r = 0 \tag{26}$$

The stress tensor components, the electric displacement vector components, the magnetic field components and the heat fluxes are determined by the following constitutive relationships:

$$\sigma_{rr} = \text{Ci}\ ]\ \pounds_{rr} + C_n{}^{\pounds}ee + \text{C}_{13}\ \pounds_{77} + d_{71}V + f_{31}\partial_z\phi - \beta_1\Theta \tag{29}$$

$$^{a}ee = \text{Ci i}\ \pounds_{QQ} + \text{C}_{12}\text{e}_{rr} + \text{C}_{13}\ \pounds_{77}\text{ -I- e}_{31}\ d_7\ V + +/_{31}\text{d^-ft0} \tag{30}$$

$$<\text{Vz} = 2C_{44}\pounds_{r7} + \text{e}_{15}\text{a}_r V - kf_{f5}d_r(/) \tag{31}$$

$$\sigma_{zz} = \text{Ci}_3\text{e}_{rr} + \text{c}_{13}\text{€00} + c^{\wedge}\pounds_{77} + \text{t-}_{33}\text{a,}\nu + +/_{33}\text{d^-ftO} \tag{32}$$

$$D_{\rho} = 2\text{e}_{15}\pounds_{r7}\text{-e}_{11}\text{a}_r\text{V-g}_{11}\text{d}_r{}^{\wedge} \tag{33}$$

$$^{\wedge}\text{z} = *31\ (^{e}\text{rr} \text{“I"}\ ^{e}ee)^{e}33^{e}?.?. \sim {}^{\epsilon}3^{\wedge}z^{V} + P_z^{sp} - g_{33}\partial_z\phi + \tau_3\Theta \tag{34}$$

$$B_r = 2/_{i}5\text{e}_{rz}\text{-g}_{11}\text{d}_r\text{V-Mn^</>} \tag{35}$$

$$^{5}\text{Z} = \text{Al}\ (^{e}\text{rr} + {}^{\pounds}ee) + /33^{e}zz\ \text{"}\quad g_{33}\partial_z V - \text{M33}^{a}\text{z}^{(/>} + \text{P3}^{0} \tag{36}$$

$$q_r = -^{\wedge}\text{IA®} \tag{37}$$

$$q_7 = -k_{33}d_7® \tag{38}$$

where, as before, C_{ij} are the elastic moduli, e_{if} are the piezoelectric coefficients, ϵ_{ij} are the permittivities, V is the (piezo) electric potential and $E_m = -dV/dz$ is the built in (piezo)electric field. Also, μ_{ij} is the permeability, $B = -\ dcfr/dz$ is the magnetic induction and cb is the magnetic potential, *fa,* r_h p,- and O are the thermal stress, pyroelec trie, pyromagnetic coefficients and temperature gradient from the reference point respectively, q_s is the heat flow and k_{ij} is the heat induction coefficient. We consider the temperature as an external parameter (for the analysis of thermo-electromechanical coupling, we refer to Ref. [29] for more details). Therefore, Eqs. (28), (37) and (38) are satisfied automatically in our wurtzite quantum dot nanostructures.

In our case we have

$$\text{err} = -\frac{dU_r}{\partial r} + \varepsilon_a^*,\quad \varepsilon_{zz} = \frac{\text{dw.}}{\partial z} + \varepsilon_c^* \tag{39}$$

$$\pounds_{ee} = -- + e_a^{U_r}\pounds_r,\quad = \frac{1}{2}\left(\frac{\partial u_r}{\partial z} + \frac{\partial u_z}{\partial r}\right) \tag{40}$$

The Rashba spin-orbit interaction and the magnetic field oriented along a direction perpendicular to the plane of 2DEG preserve the axial symmetry.[40–42] Because the total angular momentum (29) commutes With the .'-projection of the

$$j_z = l_z + \frac{\text{I}}{2}\sigma_z,\quad \text{where } l_z = -i\partial_\theta \tag{41}$$

Here, the total momentum operator, $j = \pm$l/2m and $m =$ 1,2,3.... The eigenfunctions of the total Hamiltonian operator H in (20) can be written as[4{}^2]

$$\psi_j(r,\theta,z) = \begin{bmatrix} \text{-}^{\wedge}\text{-1/2)}^{\wedge}\ z)' \\ e^{i(j-1/2)\theta}g_j(r,z) \end{bmatrix} \tag{42}$$

where $/_j$ and g_j are the components of the total wave function. The total Hamiltonian H for the conduction band can be written in cylindrical coordinates by substituting the components of (42) into (20). The details of the procedure are given in Ref. [42]. So, we can write

$$H = \begin{bmatrix} h_- & \alpha_R\left[\frac{\partial}{\partial r} + \frac{1}{r}\left(j+\frac{1}{2}\right) + \frac{eB_a r}{2\hbar}\right] \\ \alpha_R\left[-\frac{\partial}{\partial r} + \frac{1}{r}\left(j-\frac{1}{2}\right) + \frac{eB_a r}{2\hbar}\right] & h_- \end{bmatrix} \tag{43}$$

RESEARCH ARTICLE

with

$$h_{-} = \frac{ft^2}{2m_0}\left[\frac{1}{r}\frac{d}{dr}r\frac{d}{dr}\frac{1}{r^2}\frac{d}{dz}\frac{d}{dz} + \frac{1}{r^2}\frac{1}{m_e^{\perp}}\left(j \mp \frac{1}{2}\right)^2\right] + \frac{1}{2}m_e^{\perp}\omega_c^2 r^2 + \frac{\hbar\omega_c}{2}\left(j \mp \frac{1}{2}\right) + \frac{1}{2}g_0\mu_B B_z + E_g + eV + a_c(e_{zz} + e_{rr}) + e^* u_r \quad (44)$$

where $\omega_c = eB_z/m_e^{\perp}$ is the cyclotron frequency, B_z is the externally applied magnetic field along z-direction, and $m_e^{\perp}$ and $m_e^{\parallel}$ are the effective masses. Here we consider the experimentally reported bulk value $g_0 = 1.9885$ for AlN material and bulk value $g_0 = 1.9510$ for GaN material (see Ref. [66]).

The corresponding eigenvalue problem has the form

$$H|\psi_j(r, z)) = \epsilon|(A_y(r, z)) \quad (45)$$

with H in cylindrical coordinates given by (43). It satisfies the following system of second order differential equations:

$$\left(h_{-} - \epsilon\right) f_j + h_R\left[\frac{d}{dr} + \frac{1}{r}\left(j - \frac{1}{2}\right) + \frac{eB_z r}{2\hbar}\right] g_j = 0 \quad (46)$$

$$h_R\left[-\frac{d}{dr} + \frac{1}{r}\left(j + \frac{1}{2}\right) + \frac{eB_z r}{2\hbar}\right] f_j + (h_{-} - \epsilon) g_j = 0 \quad (47)$$

The differential equations (46) and (47) can be solved numerically to obtain the lowest few eigenvalues and eigenstates with respect to the various parameters. These parameters include the magnetic field B_z, mechanical strain, piezoelectric potential and piezomagnetic potential at several different temperatures (see Eqs. (24)-(38) and (44)). The analytical solution of such differential equations is available only in some special simplified cases, e.g., Ref. [42].

5. RESULTS AND DISCUSSION

Our representative examples in the study of the influence of magneto-thermo-electromechanical effects on the properties of ferroelectric, piezomagnetic and magnetoelectric QDs are the cylindrical QDs with and without wetting layers of cylindrical axial symmetry embedded into the host material as shown in Figure 1. The strain, piezoelectric field and potential profiles can be found by solving Eqs. (24)-(28) with appropriate boundary conditions. Here we apply Dirichlet boundary conditions far away from the quantum dot i.e., at the boundaries 1, 2 and 3 (see Fig. 1). Neumann boundaiy conditions have been imposed at the boundary between the quantum dot and the host material. At the center of the quantum dot i.e., at the boundary 4, the z-component of the displacement, strain, electric and magnetic potentials was set to zero.

Electron wave functions and eigenvalues are found by solving Schrodinger Eqs. (46) and (47) with appropriate boundary conditions. In particular, the electron wave functions are assumed to be zero far away from the quantum dot, implying, as mentioned above, Dirichlet boundary conditions at boundaries 1, 2 and 3. Furthermore, the electron wave functions are continuous at the boundary 4, making the choice of Neumann boundary conditions natural. The material constants for our system are listed in Table I (see also the references therein).

Our study covers the following two key cases for the QDs with and without wetting layer:

- the influence of magneto-thermo-electromechanical effects on strain, built in piezoelectric field and potential;
- the influence of magneto-thermo-electromechanical effects on the eigenstates and spin-splitting energy.

5.1. Magneto-Thermo-Electromechanical Effects in Quantum Dots with and Without Wetting Layer

In this subsection, we focus on the study of the influence of magneto-thermo-electromechanical effects on the strain, built in piezoelectric potential and piezoelectric field in cylindrical AlN/GaN and GaN/$BaTiO_3$ QDs.[20,23] For magnetic GaN/$BaTiO_3$ QDs, the material is doped (or assumed to be doped) with manganese (Mn) and we consider the material constants from Ref. [67] so that f_{if} = 0.33 N/Am and g_{ii} = 1 nano-N-s/Vc. These constants are comparable to $CoFe_2O_4$ which indicates that Mn_3GaN is a highly

reported experimental data with respect to the various parametmP^®b^®0ffP[n] anclwe TaKep$_3$ = -0.01 N/KAm, f_{yl} = 580.3 N/Am, f_{33} = 699.7 N/Am, f_{15} = 550 N/Am, g_n = 0.005 nano-N • s/Vc and g_{33} = 0.003 nano-N • s/Vc.[5:68-71] Figures 2-5 provide further insight into the influence of magneto-thermo- electromechnical effects on the strain, piezoelectric field and potentials in AlN/GaN and GaN/$BaTiO_3$ QDs with and without wetting layers.

In Figure 2, we first plot the r- and z-components of strain at r = 0 for cylindrical AlN/GaN and GaN/$BaTiO_3$ QDs without wetting layers at several temperatures. The results related to AlN/GaN QDs are consistent with those found in the literature (e.g., see Ref. [29] and references therein). They serve as a benchmark for the investigation of the influence of magneto-thermo-electromechanical effects on the properties of magnetic GaN/$BaTiO_3$ QDs. The built in strain due to lattice mismatch in AlN/GaN QDs decreases with the increase in temperature.[29] However, the influence of the thermo-electromechanical effects on the magnetic GaN/$BaTiO_3$ QDs is not as significant as for AlN/GaN QDs. Also, the r- and z-components of strain at r = 0 along z-direct!on can be enhanced significantly in GaN/$BaTiO_3$ QDs (approximately for one order of magnitude) compared to the corresponding values for AlN/GaN QDs. The variation of strain due to lattice mismatch in GaN/$BaTiO_3$ QDs along a- and c-axes is approximately —20.1% and 28.4% respectively, whereas for AlN/GaN QDs, they are —2.4% and —3.9%. It means

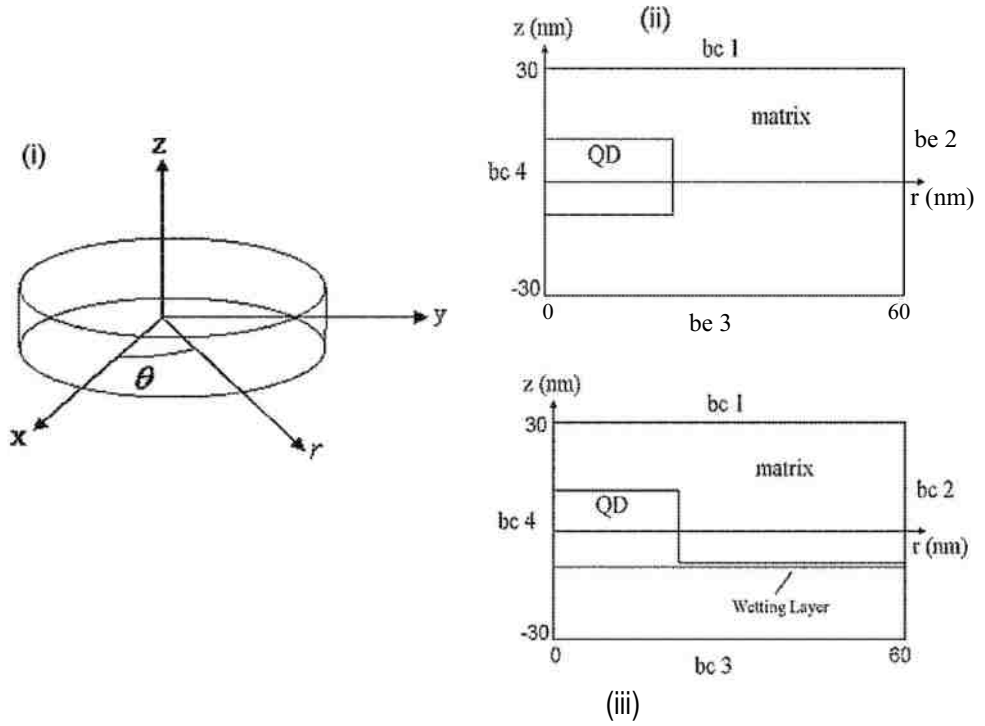

Fig. 1. The schematic diagram of the geometry of the quantum dot (see Fig. l(i)). This two dimensional cylindrical dot with and without wetting layer is shown in Figures l(ii) and (iii). The chosen geometry and size allow comparisons with the results available in the literature (see Refs. [29, 64]).

Table i. EMltMeitedn^nRidbl^iag Technology to Hniuensite de Montreal - ffibNrotfiScpes - Acquisition IPER ma8" the same as in Ref. [291, The material coHSanl^ J204)^ 84oW6tQn: ThQf'OTWfr^e 13-2^485^ along «'axis and 24.5% higher are taken from Refs. [5,68-71]. Copyright American SGlengfh&iRlilblishffirts gives the enhancement with the variation of strain in magnetic QDs.

Material constants	AIN	GaN	$BaTiO_3$
Stiffness coefficients (GPa)			
*11	396	390	166 [68]
*12	137	145	77 [68]
*1:5	108	106	78 [68]
c_{33}	373	398	162 [68]
*44	116	105	43 [68]
Permittivitty			
*11	8.67	9.28	1265 [68]
ϵ_{33}	8.57	10.02	1423 [68]
Piezoelectric coefficients (Cm^{-2})			
*15	-0.6	-0.49	11.6 [68]
*51	-0.6	-0.49	-4.4 [68]
*5:5	1.46	0.73	18.6 [68]
Pyroelectric coefficients (Cm^{-2} K^{-1})			
r_s x 10^{-6}	7.5	0.91	-19.72 [5]
Thermal stress constants (PaK^{-1})			
A_n x 10^5	-4.44	5.57	6.21 [69]
$A_{:s;s}$x 1(F	6.9	-8.66	5.51 [69]
Lattice constant (A)			
a	3.112	3.189	3.992 [70,71]
c	4.982	5.185	4.036 [70,71]
Spontaneous polarization (Cm^{-2})	-0.081	-0.029	-0.26 [20]

In Figure 3, we observe the influence of thermo-electromechanical effects on the variation of piezoelectric potential and piezoelectric field in magnetic $BaTiO_3$ QDs (See Figs. 3(ii) and (iv)). This is compared to AlN/GaN QDs (see Figs. 3(i) and (iii)). Here we do not consider the wetting layers. Again, it can be seen that the variation of potential and field with distance along z-di recti on at $r = 0$ decreases with the increase in temperature in AlN/GaN QDs and is practically independent of temperature for magnetic $BaTiO_3$ QDs. Also, it can be seen that there is a decrease in the values of the piezoelectric potential and piezoelectric field along z-di recti on at $r = 0$ in $BaTiO_3$ QDs.

In Figure 4, we examine the influence of thermo-electromechanical effects in the QDs with wetting layers. Due to the presence of wetting layers in AlN/GaN QDs, the r-component of strain at the upper interface is pushed slightly up compared to that of lower interface and vice versa for the z-component of strain. Again, the influence of the wetting layer is not significant on the electromechanical properties of magnetic GaN/$BaTiO_3$ QDs for a situation analyzed here. Figure 5 explores the influence of wetting layers on the piezoelectric potential and piezoelectric field in AlN/GaN and GaN/$BaTiO_3$ QDs at several different temperatures.

RESEARCH ARTICLE

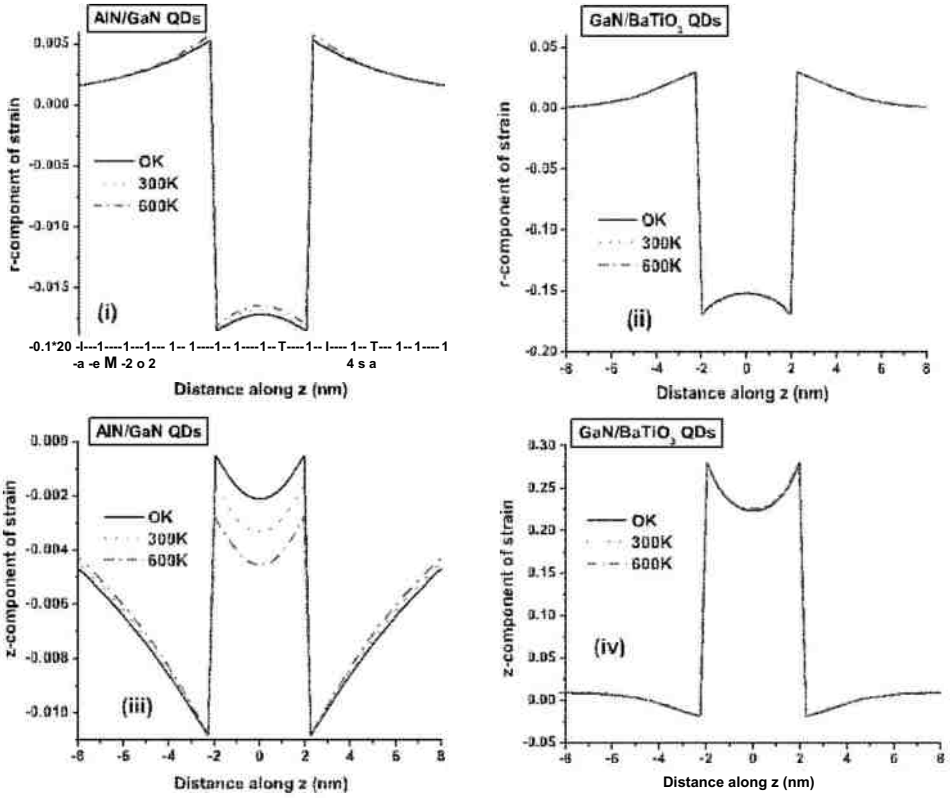

Fig. 2. The influence of thermo-electromechanical effects on the properties of cylindrical AlN/GaN and GaN/BaTiO, QDs. Upper panel represents the r-component of strain versus distance along z-direction at $r = 0$ and lower panel represents the z-component of strain versus distance along z-direction at $r = 0$. It can be seen that this component of strain in the magnetic BaTiO, QDs is independent of temperature. Here we choose $B_a = 0$.

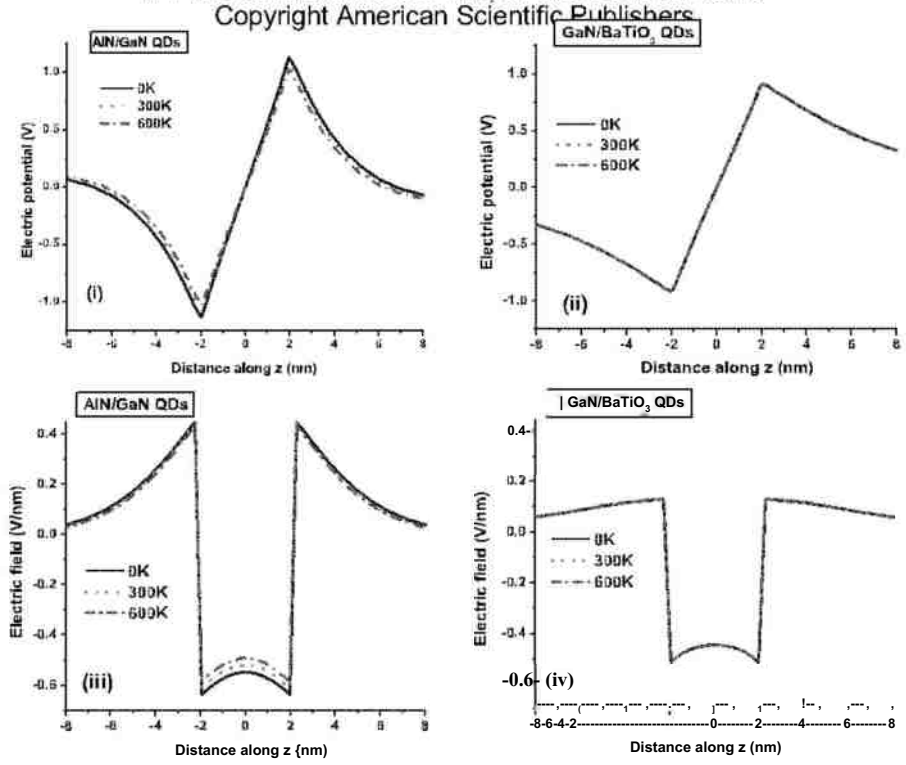

Fig. 3. The influence of thermo-electromechanical effects on the properties of cylindrical AlN/GaN and GaN/$BaTiO_s$ QDs. Upper panel represents the electric potential versus distance along z-direction at r = 0 and lower panel represents the electric field versus distance along ^-direction at r = 0. Again, it can be seen that the electric field in the magnetic $BaTiO_s$ QDs is independent of temperature. Here we choose B_a = 0.

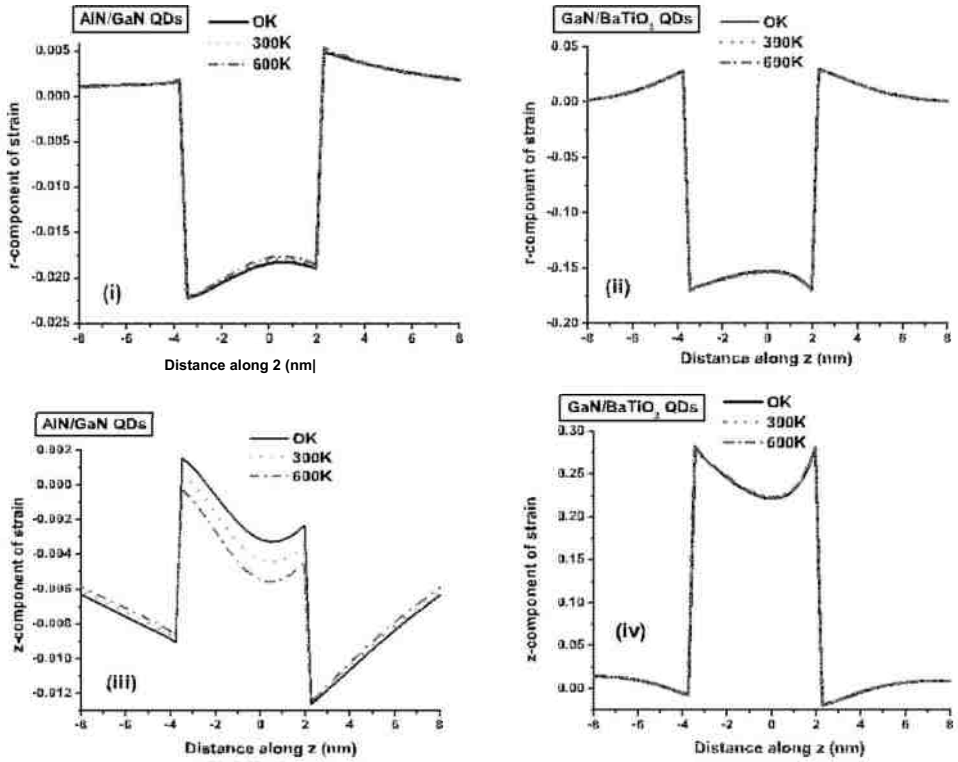

Fig. 4. The influence of wetting layers on the properties of cylindrical AlN/GaN and GaN/BaTiO, QDs. Upper panel represents the /*-component of strain versus distance along 2-direction at $r = 0$ and lower panel represents the ^-component of strain versus distance along s-direction at $r = 0$. It can he seen that the influence of wetting layers on the strain part has almost no effect for the magnetic BaTiO, QDs. Here we choose $B_a = 0$.

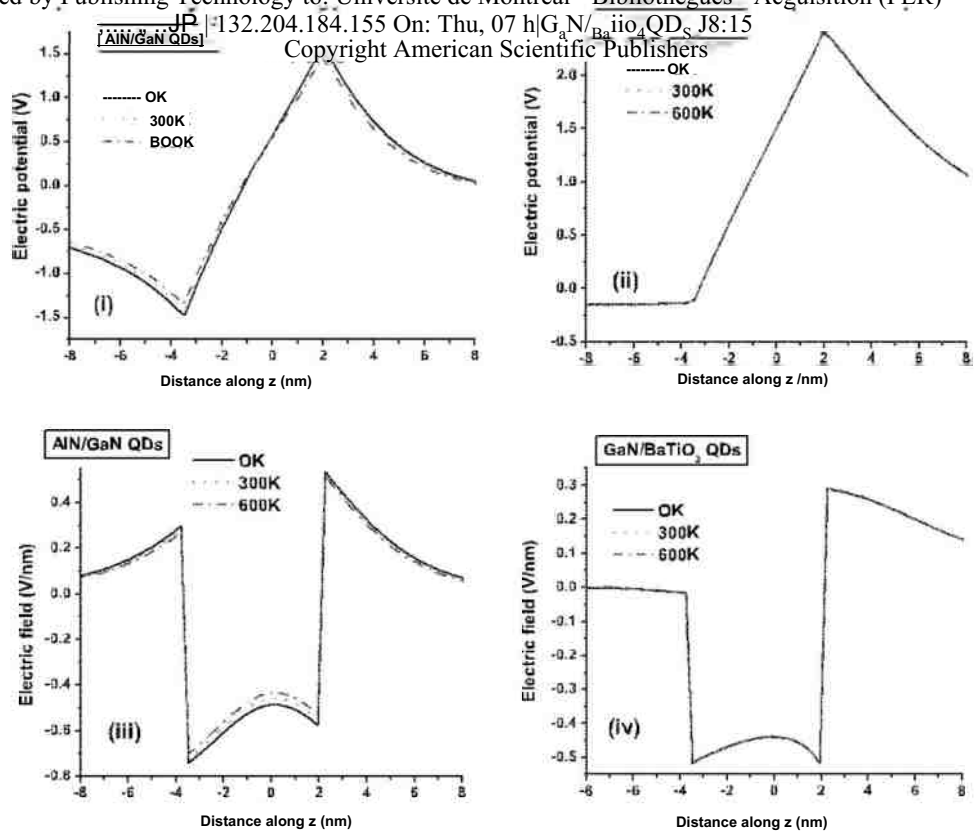

Fig. 5. The influence of wetting layers on the properties of cylindrical AlN/GaN and GaN/BaTiO, QDs. Upper panel represents the electric potential versus distance along ^-direction at $r = 0$ and lower panel represents the electric field versus distance along 3-direction at r = 0. Here we choose $B_a = 0$.

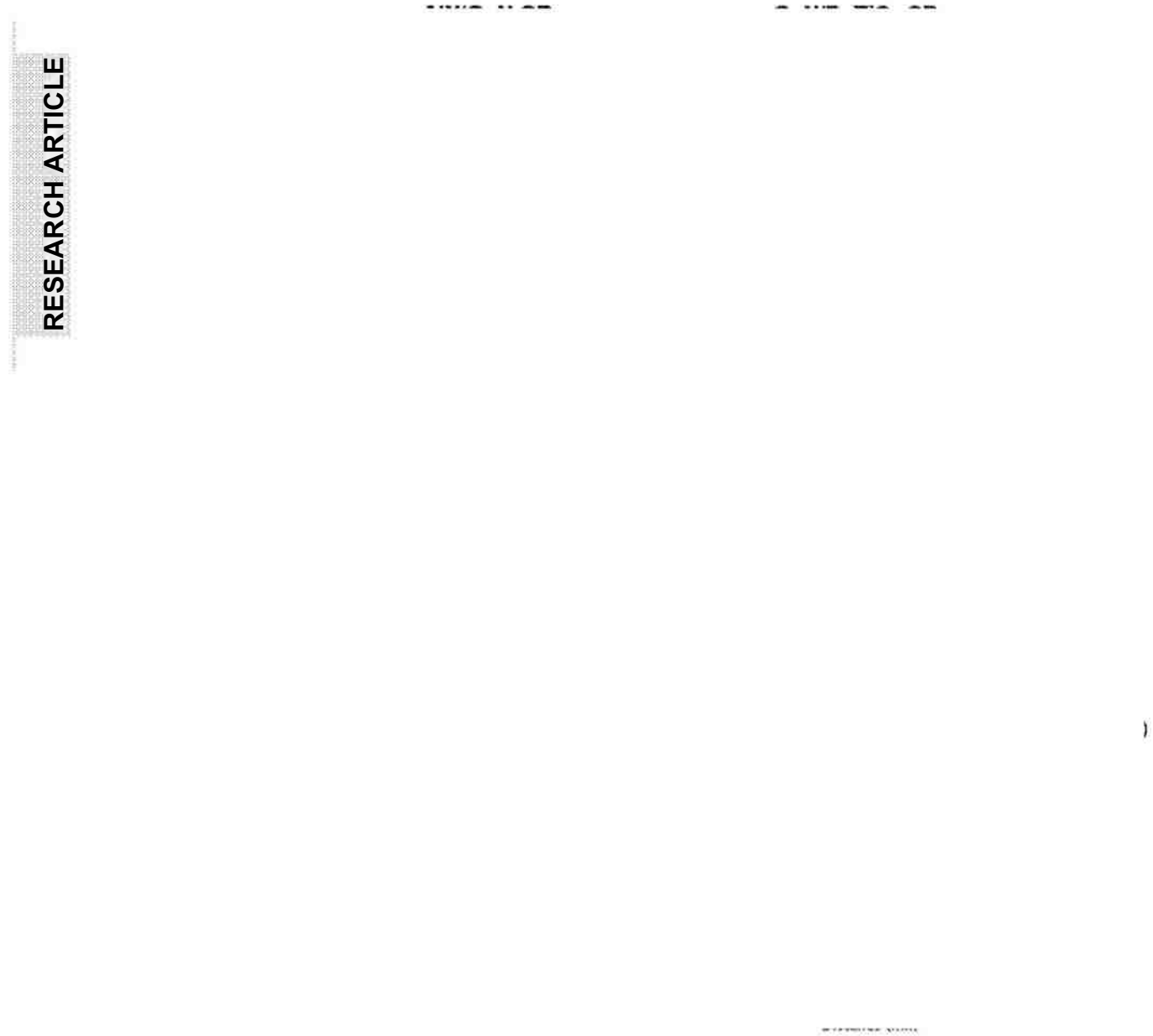

Fig- 6. The influence of electromechanical effects on the band structures of cylindrical AlN/GaN and GaN/BaTiO., QDs. Figures 5(i)-(iv) represent the ground and first excited state wave functions without the inclusion of electromechanical effects and Figures 6(v)-(vi) represent these functions with the inclusion of electromechanical effects. It can be seen that piezoelectromechanical effects bring the electron wave functions to the top of the dot. Electron wavefunctions in magnetic QDs are quite different compared to AlN/GaN QDs (see Figs. 6(v)-(viii)). Further explanations are given in the text. Here we choose $T = 0$ and $B_a = 0$.

5.2. Magnetoelectric and Piezomagnetic Quantum Dots

Next, we will highlight the results of our study on the influence of magneto-thermo-electromechanical effects in the band structure calculations of cylindrical AlN/GaN and GaN/$BaTiO_3$ QDs. The idea is to dope the materials with Mn to enhance the magnetoelectric and piezomagnetic properties of GaN/$BaTiO_3$ QDs.[67] We have also suggested to dope the GaN materials with Al so that the band gap becomes slightly larger than for $BaTiO_3$ materials. As it was pointed out before,[43] $BaTiO_3$ material can be treated in such cases as a QD.

We apply a multi-physics simulation strategy based on the finite element method[44] to provide a realistic description of the band diagram of AlN/GaN QDs. The idea is to first solve the coupled system equations of (24) through (28) in cylindrical coordinates for magnetic QDs to get the realistic electromechanical strain, piezoelectric and piezomagnetic potentials. After that, we implement the electromechanical effects in the band structure calculations of cylindrical QDs with and without wetting layers.

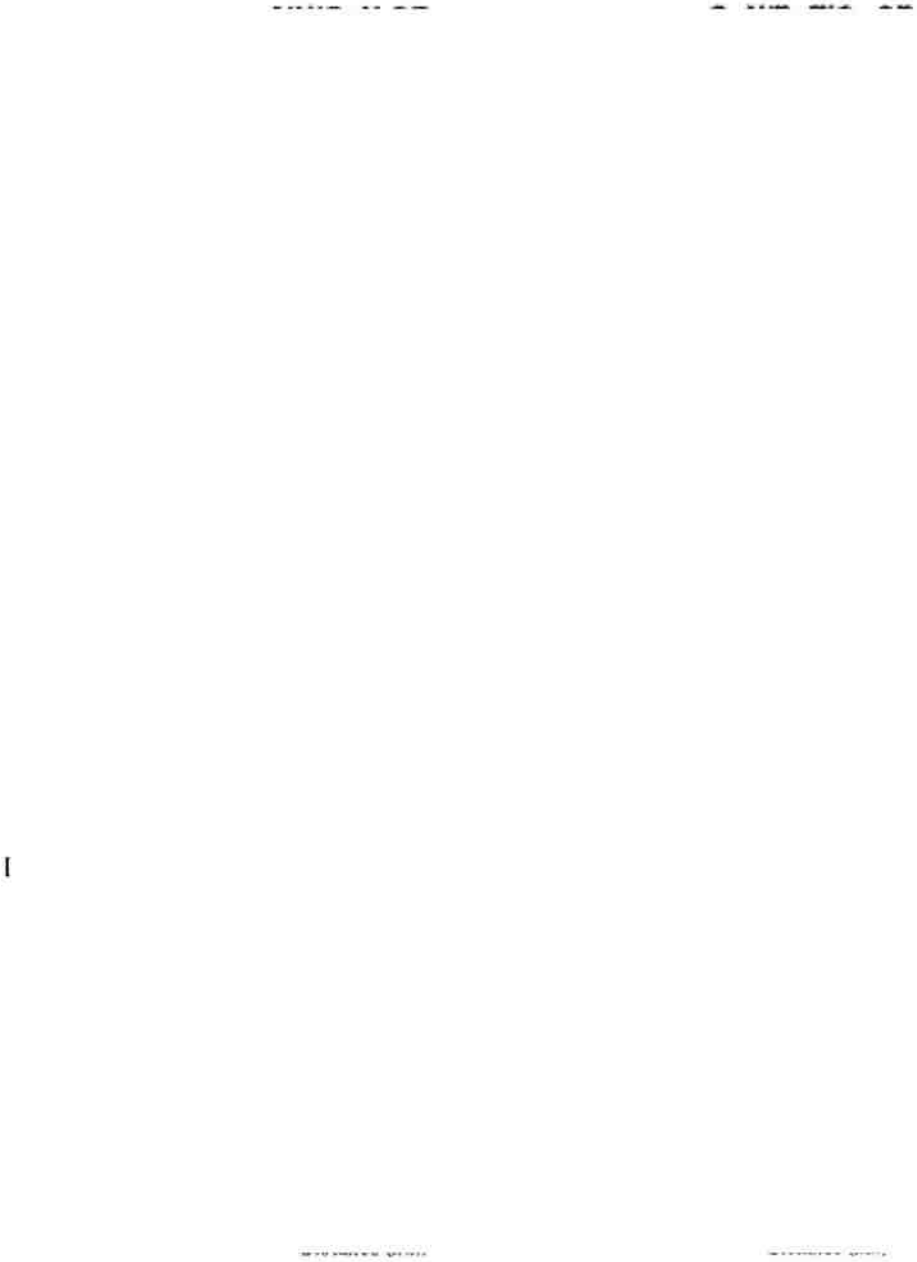

Fig. 7. The influence of electromechanical effects on the band structures of cylindrical AlN/GaN and GaN/BaTiO, QDs with wetting layers. Figures 7(i)-(iv) represent the ground and first excited state wave functions without the inclusion of electromechanical effects and Figures 6(v)-(vi) represent these functions with the inclusion of electromechanical effects. It can be seen that piezoelectromechanical effects bring the electron wave-functions to the top of the dot. Eigenvalues are found noticeably lower in magnetic QDs in the case with wetting layers (Figs. 7(vi) and (viii)) than for the case without wetting layers (Figs. 6(vi) and (viii)). Further explanations are given in the text. Here we choose $T = 0$ and $B_a = 0$.

The numerical parameters for AlN/GaN and GaN/$BaTiO_3$ QDs are taken from Refs. [29 and 43], respectively (see also references therein).

5.2.1. Influence of Magneto-Thermo-Electromechanical Effects on the Eigenstates

We add piezoelectric potential (Figs. 3(i), (ii) and 5(i), (ii)) to the flat band diagram of AlN/GaN and GaN/$BaTiO_3$ QDs and consider the combined influence of magneto- thermo-ele-ctromechanical effects as a tuning parameter in modifying the band diagram. We solve the coupled Schrödinger Eqs. (46) and (47) to get the wave functions and the eigenvalues of the QDs.

The in plane wave functions of the QDs without WLs in the flat band diagram are shown in Figures 6(i)-(iv). It can be seen that the wave functions are localized at the center of the QDs, indicating that the magneto-electromechanical effects are not accounted for in the band diagram. The influence of magneto-electromechanical effects on the

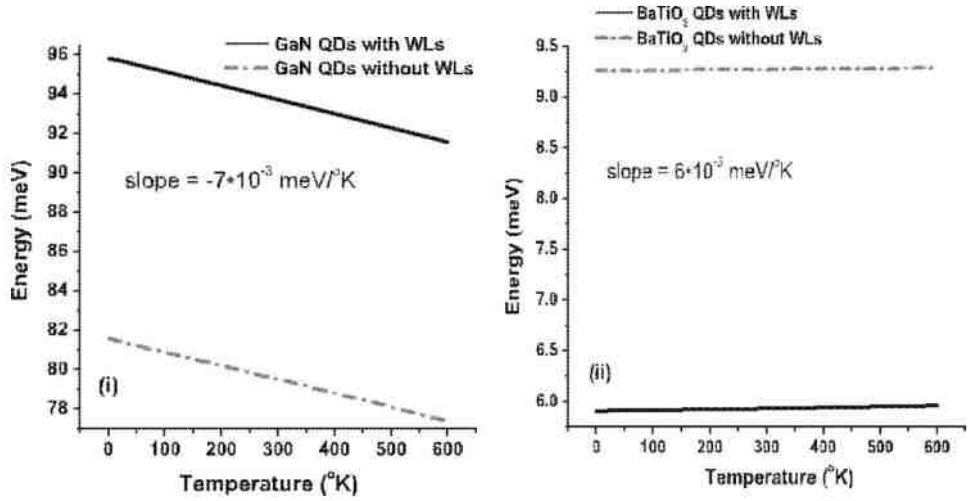

Fig. 8. Intra-subband energy difference versus temperature in GaN and $BaTiO_3$ QDs with and without wetting layers. It can be seen that in the magnetic $BaTiO_3$ QDs, the energy difference as a function of temperature is approximately two order of magnitude smaller compared to its values for GaN QDs.

wave functions and on the eigenstates are shown in Figures 6(v)-(viii). It can be seen that the influence of magneto-electromechanical effects pushed the localized wave functions to the top of the QDs. The influence of the magneto-electromechanical effects on the wave functions of the magnetic $BaTiO_3$ QDs is quite different (Figs. 6(vi), (viii)) than for GaN QDs (Figs. 6(v), (vii)). This confirms the proposal for using the magneto-electromechanical effects as a tuning parameter in controlling the localized wave functions and eigenvalues in the magnetic QDs.

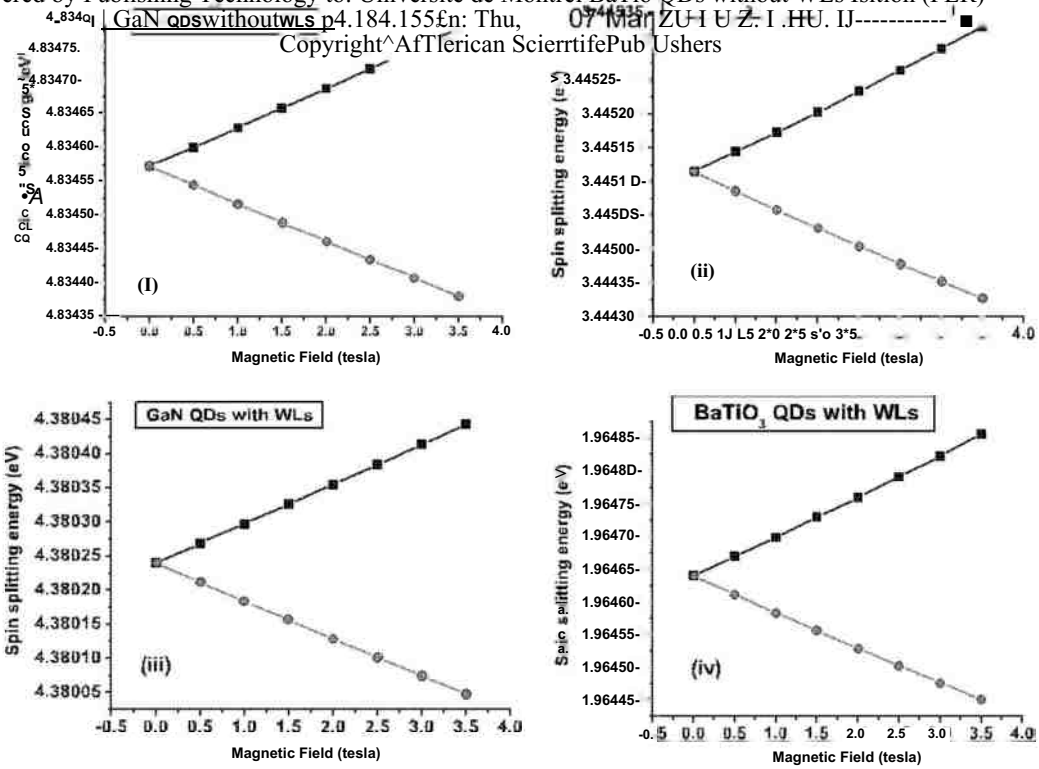

Fig. 9. The spin splitting energy between two lowest eigenstates versus magnetic field at room temperature (7' = 300 K) in AlN/GaN and GaN/$BaTiO_3$ QDs for two different cases: without WLs (Figs. 9(i), (ii)) and with WLs (Figs. 9(iii), (iv)). In Figure 9, we plotted the ground state energy of spin down electron for the quantum number j = l/2 (shown by solid lines with diamond) and ground state energy of spin up electron for the quantum number j = —1/2 (shown by solid lines with circle). Here we consider a_K = 5 x IO^{-4} eV nm as the Rashba coefficient value.

The influence of wetting layers on the eigenvalues and wave functions of the QDs are shown in Figure 7. Similar to Figure 6, the in plane wave functions of the QDs with WLs in the flat band diagram are shown in Figures 7(i)-(iv) and the influence of magneto-electromechanical effects is demonstrated in Figures 7(v)-(viii). It can be seen that the eigenvalues for the magnetic QDs with WLs are noticeably smaller (see Figs. 7(vi), (viii)) than for the case without WLs (see Figs. 6(vi), (viii)). The reason behind smaller eigenvalues in magnetic QDs with WLs is that the magneto-electromechanical effects push the flat band diagram down (Figs. 5 (ii), (iv)) in a more pronounced way than in the case without WLs (Figs. 3(ii), (iv)).

Figure 8 provides further information on the intra-subband energy (i.e., the energy difference between the ground and first excited states) versus temperature for both AlN/GaN and GaN/$BaTiO_3$ QDs with and without wetting layers. It is clear that the variation in the slope is two order of magnitude smaller in the magnetic GaN/$BaTiO_3$ QDs than in AlN/GaN QDs which indicates that the magnetic QDs are less sensitive to temperature.

5.2.2. *The Spin Splitting Energy in QDs with and without Wetting Layers*

We now turn to a presentation of another important result of this work: the spin splitting energy of ground and first excited states in AlN/GaN and GaN/$BaTiO_3$ QD^itW2ia(Wi.t1i84t'l^§tfflg: layers.

In the absence of the magnetic field, as it is clear from (43), there is an additional asymmetry at j_7 -> — / due to the time inversion. It means that the eigenstates with the projection of total angular momentum equal to j and — j are Kramer's degenerate. In Figures 9(i), (ii), we find the ground state Kramer's degenerate eigenvalues at 4.83 eV for AlN/GaN QDs and 3.44 eV for GaN/$BaTiO_3$ QDs without wetting layers. These results have been obtained by directly solving the coupled Schrödinger Eqs. (46) and (47). Here we consider j = 1 /2 in Eq. (46) and —j—i /2 in Eq. (47). In the presence of magnetic field along ^-direction, there is no degeneracy and we obtain the spin splitting energy. In the presence of wetting layers in the QDs (Figs. 9(iii), (iv)), Kramer's degenerate eigenvalues and spin splitting energy occur at lower values. We found that the divergence in the Zeeman spin splitting energy increases with the increase in magnetic field due to the Rashba spin-orbit coupling in both cases: QDs with wetting layers and without wetting layers.

Finally, in Figure 10, we plotted the spin spirited energy difference of the ground and first excited states versus magnetic field in the QDs. Here we solved the Schrödinger Eqs. (46) and (47) to get the ground state eigenvalues for j = 1/2 and j = —1/2. We keep the Rashba coefficient value at a_R = 5 x 10^{-4} eV nm. There is a slight variation in the spin splitting energy difference versus magnetic field

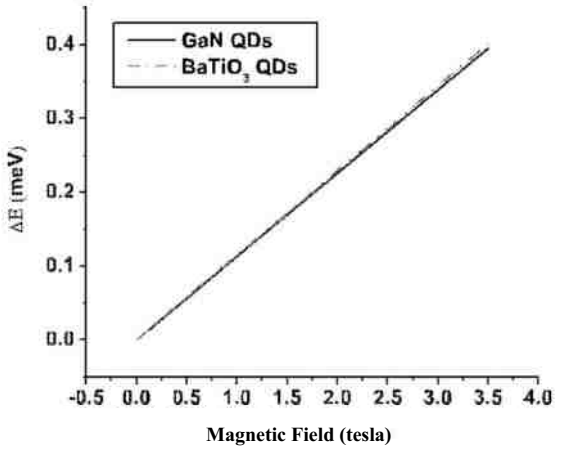

Fig. 10. The spin splitting energy difference versus magnetic field of AlN/GaN (solid line) and GaN/$BaTiO_3$ (dashed-dotted line) QDs at room temperature (i.e., at T = 300 K).

in magnetic $BaTiO_3$ compared to GaN QDs. The spin splitting energy difference is controlled by the Zeeman term ($g_O$jii_BBtr$_7$, see Eq. (21)) and it is increased with the increase in the magnetic field. However, the variation in the spin splitting energy difference between GaN and $BaTiO_3$ QDs is mainly due to the variation in the bulk value of g-factor. Note that the bulk g-factor for GaN material is 1.95[66] and for $BaTiO_3$, we consider free electron g-factor i.e., 2.

6. CONCLUSIONS

We have carried out a systematic study of the influence of the magneto-thermo-electromechanical effects on the properties of QDs with and without WLs. In this study, we have covered three different groups of nanostructures such as ferroelectric, piezomagnetic and piezoelectric QDs.

Firstly, we have analyzed in detail the influence of magneto-thermo-electromechanical effects on the strain, electric field and electric potential of cylindrical AlN/GaN and GaN/$BaTiO_3$ QDs with and without wetting layers. We have shown (see Figs. 2, 4) that the ^-components of strain at r = 0 along ^-direction can be enhanced significantly due to higher lattice mismatch along ^-direction for ferroelectric QDs compared to piezoelectric QDs. Also, piezoelectric and stiffness coefficients of ferroelectric QDs are much smaller than their counterparts in piezoelectric QDs. This causes a decrease in electric potential and electric field for ferroelectric QDs in comparison to piezoelectric QDs (see Figs. 3, 5).

Secondly, we have analyzed the influence of magneto-thermo-electromechanical effects on the band structures of cylindrical AlN/GaN and GaN/$BaTiO_3$ QDs with and without wetting layers (see Figs. 6-8). While it has been demonstrated that the wetting layer has a significant effect on the modification of strain, electric field and electric potential, we have also demonstrated that it modifies the

band diagram and localized eigenstates of the QDs. Furthermore, we have accounted for the magneto-thermo-piezoelectric effect in the band structure of magnetic QDs in the presence of spin-orbit interaction and employed a fully coupled numerical approach to obtain the eigenvalues and eigenstates based on the finite element method.

Finally, as demonstrated by Figures 9 and 10, we have carried out a numerical simulation study of the spin splitted energy in magnetic AlN/GaN and GaN/$BaTiO_3$ QDs with and without WLs. We have shown that in the presence of externally applied magnetic field along z-di recti on, the spin splitting energy in magnetic QDs with WLs can be shifted significantly to the lower energy levels in magnetic QDs with WLs.

Acknowledgments: This work was supported by the Ikerbasque, Spain, the University of Jyväskylä, Finland and by the NSERC and CRC program, Canada.

References

1. R. M. Abolfath, A. G. Petukhov, and I. Zutic, *Phys. Rev. Leu.* 101, 207202 **(2008).**
2. R. de Sousa and J. E. Moore, *Phys. Rev. B* 77, 012406 **(2008).**
3. I. Apostolova and J. Wesselinowa, *Solid State Commun.* 147, 94 **(2008).**
4. F. Zavaliche, H. Zheng, L. Mohaddes-Ardabili, S. Y. Yang, Q. Zhan, P. Shafer, E. Reilly, R. Chopdekar, Y. Jia, P. Wright, D. G. Schlom, ■vc i ■ J >
5. W. J. Feng, E. Pan, and X. Wang, *J. Appl. Phys.* 103, 063705 (2008). **31,497 (2008). ~ ....** Copyright American Scie^icJ^bli^^oofi).
6. R. de Sousa and S. D. Sarma, *Phys. Rev. B ,* 68 5 30 **(2003).**
7. S. Prabhakar and J. E. Raynolds, *Phys. Rev. B* 79, 195307 **(2009).**
8. S. Prabhakar and R. Melnik, *./. Appl. Phys.* 108, 064330 **(2010).**
9. S. Prabhakar, J. Raynolds, A. Inomata, and R. Melnik, *Phys. Rev. B* 82, 195306 **(2010).**
10. S. M. Reimann and M. Manninen, *Rev. Mod. Phys.* 74, 1283 **(2002).**
11. A. L. Efros, E. I. Rashba, and M. Rosen, *Phys. Rev. Leu.* 87, 206601 **(2001).**
12. M. Bahram i-S am an i, S. R. Patil, and R. Melnik,*Phys.: Condens. Mauer* 22, 495301 (2010).
13. E. Takhtamirov and R. V. N. Melnik, *New Journal of Physics* 12, 123006 **(2010).**
14. S. Prabhakar, J. E. Raynolds, and R. Melnik, *Phys. Rev. B* 84, 155208 **(2011).**
15. S. Prabhakar, R. V. N. Melnik, and L. L. Bonilla, *Appl. Phys. Leu.* 100, 023108 **(2012).**
16. S. Y. Wu, H. X. Liu, L. Gu, R. K. Singh, L. Budd, M. van Schilfgaarde, M. R. McCartney, D. J. Smith, and N. Newman, *Appl. Phys. Leu.* 82, 3047 **(2003).**
17. S. Selvan, P. Patra, C. Ang, and J. Ying, *Angewandte Chemie* 119, 2500 **(2007).**
18. T. Graf, M. Gjukic, M. S. Brandt, M. Stutzmann, and O. Ambacher, *Appl. Phys. Leu.* 81, 5159 (2002).
19. E. Kulatov, **H.** Nakayama, **H.** Mariette, **H.** Ohta, and Y. A. Uspenskii, *Phys. Rev. B* 66, 045203 **(2002).**
20. Y.-R. Wu and J. Singh, *Appl. Phys. Leu.* 85, 1223 **(2004).**
21. **H.** Fu and L. Bellaiche, *Phys. Rev. Leu.* 91, 257601 **(2003).**
22. W. Eerenstein, N. **D.** Mathur, and J. F. Scott, *Nature* 442, 759 **(2006).**
23. Z. Wang, J. Hu, A. P. Suryavanshi, K. Yum, and M.-F. Yu, *Nano Leu. 1,* 2966 (2007).
24. L. Huang, Z. Jia, I. Kymissis, and S. O'Brien, *Adv. Runet. Mater.* 20, 554 **(2010).**
25. **B.** Lorenz, A. P. Litvinchuk, M. M. Gospodinov, and C. W. Chu, *Phys. Rev. Leu.* 92, 087204 **(2004).**
26. Y. G. J. Akimoto and Y. Oosawa, *Crystal Structure Communications* C50, 160 (1994).
27. S. R. Patil and R. V. N. Melnik, *J. Phys. D: Appl. Phys.* 42, 145113 **(2009).**
28. R. V. N. Melnik and R. Mahapatra, *Computers and Structures* 85, 698 **(2007).**
29. S. R. Patil and R. V. N. Melnik, *Nanotechnology* 20, 125402 **(2009).**
30. R. V. N. Melnik and M. Willatzen, *Nanotechnology* 15, 1 **(2004).**
31. R. V. N. Melnik and K. N. Zotsenko, *Modelling and Simulation in Materials Science and Engineering* 12, 465 **(2004).**
32. J. E. Rolon and S. E. Ulloa, P/m. /feu *B* 79, 245309 **(2009).**
33. A. Schliwa, M. Winkelnkeniper, and D. Bimberg, *Phys. Rev. B* 76, 205324 **(2007).**
34. C. Kindel, S. Kako, T. Kawano, **H.** Oishi, Y. Arakawa, G. Honig, M. Winkelnkeniper, A. Schliwa, A. Hoffmann, and D. Bimberg, *Phys. Rev. B* 81, 241309 **(2010).**
35. T. Warming, E. Siebert, A. Schliwa, E. Stock, R. Zimmermann, and **D.** Bimberg, *Phys. Rev. B* 79, 125316 **(2009).**
36. Y. A. Bychkov and E. I. Rashba/. *Phys. C: Solid State Phys.* 17, 6039 **(1984).**
37. E. I. Rashba and A. L. Efros, *Phys. Rev. Lett.* 91, 126405 **(2003).**
38. A. V. Khaetskii, *Phys. Rev. B* 45, 13777 **(1992).**
39. C. F. Destefani and S. E. Ulloa, *Phys. Rev. B* 71, 161303 **(2005).**
40. J. Y. Fu and M. W. Wu,./. *Appl. Phys.* 104, 093712 **(2008).**
41. W. **H.** Kuan, C. S. Tang, and W. Xu,,/. *Appl. Phys.* 95, 6368 **(2004).**
42. E. Tsitsishvili, G. S. Lozano, and A. O. Gogolin, *Phys. Rev. B* 70, 115316 **(2004).**
43. J. Zhang, C. Yang, S. Wu, Y. Liu, **H.** Chen, W. Zhang, and Y. Li, *Appl. Phys. Leu.* 95, 122101 **(2009).**
44. Comsol Multiphysics version 3.5a (www.comsol.comL.
45. W. Jakoboski, M. Zielinsk ?, G. W. Bryant, and J. Aizpurua, *Phys.*
46. *Appl. Phys. Lett.* 72,3109 (1998).
47. R. Santoprete, B. Koiller, R. B. Cap az, P. Kratzer, Q. K. K. Liu, and M. Scheffler, *Phys. Rev. B* 68, 235311 **(2003).**
48. G. Bester, J. Shumway, and A. Zunger, *Phys. Rev. Leu.* 93, 047401 **(2004).**
49. R. V. N. Melnik, *Comput. Phys. Commun.* 142, 231 **(2001).**
50. R. V. N. Melnik, *International Communications in Heat and Mass Transfer* 30, 83 **(2003).**
51. R. Melnik, B. Lassen, L. L. Y. Voon, M. Willatzen, and C. Galeriu, *Nonlinear Analysis: Theory, Methods and Amp: Applications* 63, e2165 **(2005).**
52. B. Lassen, R. Melnik, M. Willatzen, and L. L. Y. Voon, *Nonlinear Analysis: Theory, Methods and amp: Applications* 63, el607 **(2005).**
53. B. Lassen, M. Willatzen, and R. Melnik,./. *Comput. Theor. Nanosci.* 3, 588 **(2006).**
54. **B.** Lassen, M. Willatzen, R. Melnik, and L. C. L. Y. Voon, *Journal of Mathematical Physics* 46, 112102 **(2005).**
55. R. V. N. Melnik,.*Applied Mathematics and Computation* 107,27 **(2000).**
56. X. Peng and P. Logan, *Appl. Phys. Leu.* 96, 143119 **(2010).**
57. I. M. Lifshits and L. N. Rozentsveig, *Zh. Eks. Tear. Eiz.* 17, 783 **(1947).**
58. F. C. Buroni and A. Saez, *Proc. R. Soc. A* 466, 515 **(2010).**
59. G. Bir and G. Pikus, Symmetry and Strain Induced Effects in Semiconductors, John Wiley & Sons, Inc., New York **(1974).**
60. C. Pryor, *Phys. Rev. B* 57, 7190 **(1998).**
61. T. Andlauer, R. Morschl, and P. Vogl, *Phys. Rev. B* 78, 075317 **(2008).**
62. T. Andlauer and P. Vogl, P/m. *Rev. B* 79, 045307 **(2009).**
63. P. Tan and L. Tong, *Composites Part A: Applied Science and Manufacturing* 33, **631 (2002).**
64. B. Lassen, M. Willatzen, D. Barettin, R. V. N. Melnik, and L. C. L, Y. Voon, *Journal of Physics: Conference Series* 107, 01 **(2008).**

65. P.-F. Hou, T. Yi, and L. Wang, *Journal of Thermal Stresses* 31, 807 **(2008).**
66. M. W. Bayed, M. S. Brandt, T. Graf, O. Ambacher, J. A. Majewski, M. Stutzmann, D. J. As, and K. Lischka, *Phys. Rev. B* 63, 165204 **(2001).**
67. P. Lukashev, R. F. Sabirianov, and K. Belashchenko, *Phys. Rev. B* 78, 184414 **(2008).**
68. J. **H.** Huang and W.-S. Kuo, *J. Appl. Phys.* 81, 1378 **(1997).**
69. P.-F. Hou, G.-H. Teng, and H.-R. Chen, *Meeh. Mater.* 41, 329 **(2009).**
70. L. **B.** Stephen O'Brien and C. **B.** Murray, *J. Am. Chem. Soc.* 123, 12085 **(2001).**
71. **H.** Zheng, J. Wang, S. E. Lofland, Z. Ma, L. Mohaddes-Ardabili, T. Zhao, L. Salamanca-Riba, S. R. Shinde, S. B. Ogale, F. Bai, D. Viehland, Y. Jia, D. G. Seldom, M. Wuttig, A. Roytburd, and R. Ramesh, *Science* 303, 661 **(2004).**

Received: 27 December 2011. Accepted: 29 January 2012.